An on-line chromatic and scale-space microvasculature-tracing analysis for transmitted light optical images

Constantino Carlos Reyes-Aldasoro[1,2], Meit A. Björndahl[1], Simon Akerman[1], Jamila Ibrahim[1] and Gillian M. Tozer[1]
http://tmg.group.shef.ac.uk

1 Cancer Research UK Tumour Microcirculation Group, Oncology, The University of Sheffield, S10 2RX.
2 Biomedical Engineering Group, University of Sussex, Brighton, BN1 9RH.

Abstract

Limited contrast in optical images from intravital microscopy is problematic for analysing tumour vascular morphology. Moreover, in some cases, changes in vasculature are visible to a human observer but are not easy to quantify. In this paper two quantitative on-line algorithms are presented: scale-space vessel tracing and chromatic decomposition for tumour vasculature from in-vivo transmitted light optical images. The algorithms were tested on intravital window chamber images of the vasculature from SW1222 human colorectal carcinomas, which were treated with a vascular disrupting agent combretastatin-A-4-phosphate (CA-4-P) or saline. The results confirmed the well-known effects of CA-4-P on the constriction of vessels. Furthermore, changes in the chromaticity suggest a deoxygenation of the blood with a recovery to initial levels in CA-4-P-treated tumours relative to the controls. The algorithms can be freely applied to any vascular image through the CAIMAN (CAncer IMage ANalysis: http://www.caiman.org.uk).
Keywords: vessel tracing, chromatic analysis, tumour vasculature.

1 Introduction

Quantitative analysis of microvascular images is important in a number of biomedical applications; in cancer, the tumour vasculature is emerging as an important therapeutic target [7]. In understanding the development of the vasculature and the action of vasoactive drugs, a quantification of vascular structures and its variation is crucial. Vascular changes can be observed either through topology (number, size, distribution of the vessels), chromatic characteristics, or other functional parameters (red blood cell velocity for instance).

The chromatic channels Hue, Saturation and Value (*HSV*) provide higher discrimination that the traditional Red, Green and Blue (*RGB*) channels [4, 5]. The *HSV* colour model describes perceptual colour relationships related to the artistic ideas of hue, tint and shade. Histograms of colour images have been used as 1D/2D/3D histograms of separate channels (*RGB* or *HSV*) for segmentation, histogram equalisation, or image enhancement [5].

To observe the topology of the tumour vasculature, besides manual tracing of the vessels, which is a long and subjective process, several algorithms [1, 2, 10] have been proposed.

Some of these algorithms require manual verification of the vessels or require a difference of intensities between the vessels and the background, such as those obtained from multiphoton microscopy, which is not always possible in the case of light microscopy.

For this work, we generated a 3D chromatic histogram as described in [5] and followed the centroids of the clouds corresponding to the image chromaticity in time. We also implemented a scale-space ridge detection algorithm [3] as a fully automatic vessel tracing algorithm. Both algorithms were implemented on a website called *CAIMAN* [6] and are freely accessible.

2 Material and methods

SW1222 human colorectal carcinoma cells were implanted into window chamber-bearing mice under anaesthesia [9], for intravital microscopy to monitor vascular growth and development. 96 transmitted light images (x10 objective) were acquired from 4 restrained window chamber-bearing mice: CA-4-P treated (n=3) or control (saline treated, n=3) in 2 regions of interest (centre and periphery of tumour) before (time=0) and up to 24h (2.5, 15, 30, 60, 180, 360, 1440 min) after treatment with 30 mg/kg of CA-4-P or saline.

3 Algorithm definition

In this work, we considered that a colour image I_{rgb} had dimensions $N_r \times N_c \times 3$ for rows, columns and three colour channels $[R,G,B]$ red, green and blue. Hue, $h \in [0,360^\circ]$, is a circular property related to the wavelength of the colour where red corresponded approximately to 0°, yellow to 60°, green to 120°, cyan to 180°, blue to 240° and magenta to 315°. The saturation $s \in [0,1]$, is a measure of the purity of the colour or its departure from white or grey and value $v \in [0,1]$, is a measure of the brightness.

The hue-saturation-value histogram is a tri-variate measurement of the relative frequency of the chromatic characteristics of the image and it was defined [5] as: $m_{HSV}\ (h,s,v) = \frac{\#\{x \in (L_r \times L_c) : I_{hue}(x)=h,\, I_{sat}(x)=s,\, I_{val}(x)=v\}}{\#\{L_r \times L_c\}}$, where # denoted the number of elements in the set, $L_r = \{1,2,\ldots,r,\ldots,N_r\}$, $L_c = \{1,2,\ldots,c,\ldots,N_c\}$, and $x \in (L_r \times L_c)$ describe the spatial domains of the data. Fig 1 shows a time line of the vasculature of a tumour as I_{rgb} and m_{HSV}. To represent the frequency in 3D, spheres of sizes according to their number of elements are plotted at the HSV space with their corresponding colours.

The vasculature was traced with a scale-space algorithm [3], which is a multiscale technique in which a progressive filtering or smoothing is applied to an image with the intention of detecting features (ridges, edges, blobs, etc.) of different dimensions at different scales. The centreline of vessels was detected as a *ridge* in a topographical analogy. The scale-space representation of a function $f(r,c)$ can be defined as the convolution with a Gaussian $g(r,c;t)$ where t corresponds to the width of the Gaussian: $L(r,c;t) = g(r,c;t) * f(r,c) = \frac{1}{(2\pi t)} e^{-(r^2+c^2)/(2t)} * f(r,c)$.

Then, the normalised first and second derivatives in r and c dimensions (Lr, Lrr, Lc, Lcc), which form the Hessian Matrix H, highlighted the rate of change of the intensities of the images. Regions of maxima and minima were calculated when the derivatives reached zero. To obtain the centrelines of vessels, or ridges, it was necessary to convert from the (r,c) coordinate system to a local (p,q) system aligned with the eigendirections of H: $L_p = \partial_p L = (\sin\beta\ \partial_x - \cos\beta\ \partial_y)L$, $L_q = \partial_q L = (\cos\beta\ \partial_x + \sin\beta\ \partial_y)L$, $L_{pq} = \partial_p \partial_q L = (\cos\beta\ \partial_x +$

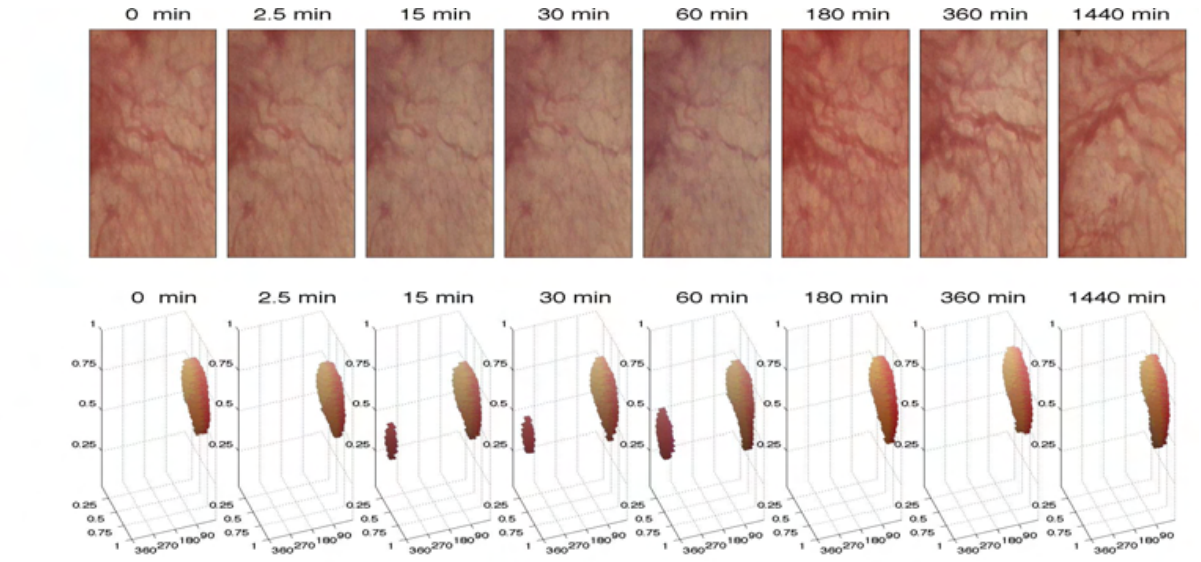

Figure 1: Chromatic variation of a tumour with time. Eight time points of the vasculature (top) and their corresponding 3D m_{HSV} histograms (bottom). Notice the drift of the cloud in the first 60m and the change at 3h.

$\sin\beta\ \partial_y)(\sin\beta\ \partial_x - \cos\beta\ \partial_y)L$, where β denotes the angle of rotation of the coordinate system and it was defined by: $\cos\beta|_{(x_o,y_o)} = \sqrt{\frac{1}{2}\left(1+\frac{L_{xx}-L_{yy}}{(L_{xx}-L_{yy})^2+4L_{xy}^2}\right)}\Bigg|_{(x_o,y_o)}$, $\sin\beta|_{(x_o,y_o)} = (sign\ L_{xy}) \times \sqrt{\frac{1}{2}\left(1-\frac{L_{xx}-L_{yy}}{(L_{xx}-L_{yy})^2+4L_{xy}^2}\right)}\Bigg|_{(x_o,y_o)}$. The ridges at different scales constituted a scale-space ridge surface and were defined as the points of (Lp, Lpp, Lq, Lqq) that fulfilled the conditions of maxima at every scale. Finally, a *scale space ridge* was simplified from the ridge surface by selecting the points where the surface had maximal values by a given norm. Thus, fine ridges were detected at fine scales whilst coarse ridges had higher norm values at larger scales. The detected scale space ridges were ranked by the saliency of the ridge, which indicates which ridges are better defined in the contrast between the ridge itself and the surrounding regions. The *saliency* is calculated as the integration of the edge strength over the ridge and the *edge strength* is derived from the magnitude of the gradient $(L_x^2 + L_y^2)$ at each point.

4 Results and Discussion

The 96 images were processed through CAIMAN. The chromatic analysis algorithm produced m_{HSV} from which the centroid of the cloud was obtained for H, S, and V. Fig. 1 shows the time course of the tumour images (top row) and their corresponding 3D histograms (bottom row). It should be noted how the cloud shifts in H (a small cloud appears on the left side at 15 min) as well as in S and V (cloud moves "forward" and down). At 3h there is a change in colour noticeable by the disappearance of the contraction of the cloud on the left.

Fig. 2 shows an illustrative example of vessel tracing. The output of the algorithm consisted of an image with ridges overlaid (Fig. 2b), a matrix with the ridges (Fig. 2c) and a series of measurements. For this paper we analysed average vessel length, average vessel diameter and vessel density. These measurements were calculated for all ridges and for the

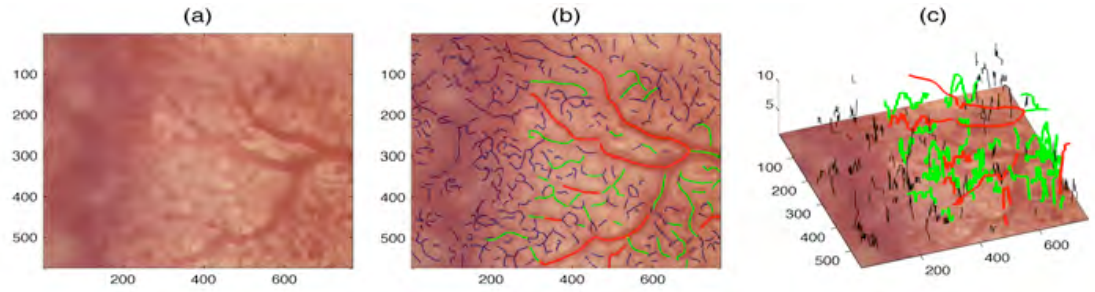

Figure 2: Vasculature tracing by scale-space. The algorithm detected vessels in an analogy to topological ridges at different scales, selected the optimal scale and then ranked them according to the saliency (a) Original window chamber image. (b) Ridges overlaid on the original image. Ten most salient ridges are labelled in red, the next 40 in green and the rest in black. (c) The ridges as a 3D structure.

10 ridges with a higher saliency, i.e. the most important ones according to the algorithm (labelled in red in Fig. 2c).

The algorithm detected 355 ridges with average lengths and widths of 31.9 and 10.1 pixels respectively. The corresponding measurements for the 10 most salient ridges (Fig. 2b red lines) were 127.6 and 15.1, which indicated that the most salient ridges were considerably longer and wider than the rest (green and black lines). The 50 most salient ridges concentrated on the right side of the image where the vasculature was well defined, but ridges were also detected in the left side. The scale of detection is illustrated in Fig. 2c where the z-axis corresponds to the scale; the height is proportional to the width of the vessels as it can be seen from the two long red lines in the centre of the image. For clarity only some of the black lines were plotted. It is important to notice that the two methods are independent of each other, that is, the chromatic characteristics do not have any relationship with the tracing.

The temporal effects of the vascular disrupting agent CA-4-P were analysed for 6 measurements (Fig. 3). The lines have been normalised by removing the mean and divided by the standard deviation of the sample values. Blue lines with round markers correspond CA-4-P treated tumours, while red lines with x markers correspond to saline.

While the length and width remained constant after treatment with saline (Fig. 3a,b), the length of the vessels treated with CA-4-P decreased considerably up to 60 min after treatment with a subsequent recovery. The density of vessels remained constant for both groups. These effects corresponded with the well-known constriction effect of CA-4-P [8].

The chromatic analysis revealed a small shift in H during the first minutes from red towards yellow returning to the initial values around 60 min. Then, around 3h, the CA-4-P group presented a significant drop towards deep-red, purple, with a subsequent recovery, while saline remained closer to the initial values. A similar variation was detected for S, where the saline group remained constant throughout the time course but the CA-4-P presented a decrease in saturation (i.e. towards white) up to 60 min, with a considerable reverse at 3h and a further return to the initial values. These trends were not detected for V.

The decrease of length and diameter must imply a reduction of the flow in the tumour and a subsequent deoxygenation of the tissue, which in turn explains the drop in saturation shown in Fig. 3e. Then, the jump at 3h of S and H should correspond to a recovery of the vasculature and an increased blood flow, that later stabilised to the original levels.

These algorithms can be applied to images on-line, without the need to perform any

programming, thus enabling researchers to perform quantitative analysis of data that would traditionally be analysed by visual examination.

This work was funded by Cancer Research UK.

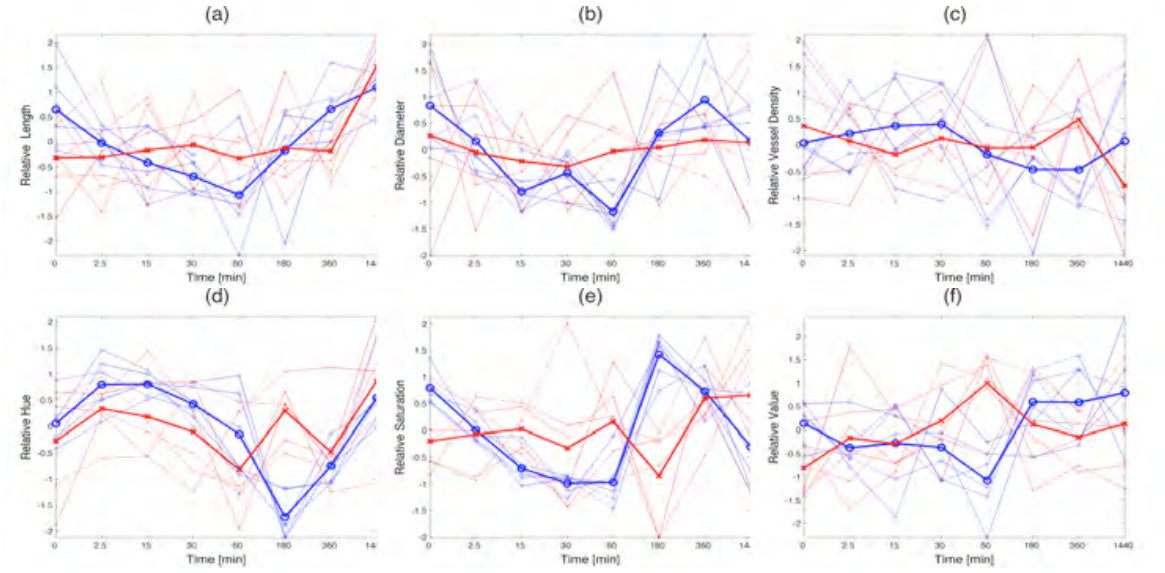

Figure 3: Vascular and chromatic measurements: (a) length, (b) diameter, (c) vessel density (d) hue, (e) saturation, (f) value. Saline = x marker red line, CA-4-P = round marker blue line. Thick lines indicate the average of each group per time point. Notice how the vessel diameters and lengths of the saline group remained constant while CA-4-P induced a decrease up to 1h, after which vessels recovered. The vessel density of both groups remained constant with time. Hue shifted towards yellow and then to red around 3h in CA-4-P and saturation decreased up to 1h with a drastic increase at 3h later to recover. Value remained constant.

References

[1] **M. A. Abdul-Karim** *et. al.* **. Automated tracing and change analysis of angiogenic vasculature from in vivo multiphoton confocal image time series.** ***Microvasc Res*****, 66(2):113–25, 2003.**

[2] **P. R. Barber** *et. al.* **. Semi-automated s/w for 3d delineation vascular n.** ***J Micros*****, 211(P 1):54–62, 2003.**

[3] **T. Lindeberg. Edge detection and ridge detection.** ***Int J of Comp Visi*****, 30(2):117–154, 1998.**

[4] **O. A. Maximova** *et. al.* **. Computerized morphometric analysis of pathological prion protein deposition in scrapie-infected hamster brain.** ***J. Histochem. Cytochem.*****, 54(1):97–107, 2006.**

[5] **C. C. Reyes-Aldasoro** *et. al.* **. An automatic segmentation algorithm for the morphological analysis of microvessels in immunostained histological tumour sections.** ***J Microsc*****, 2011.**

[6] **C. C. Reyes-Aldasoro** *et. al.* **. Caiman: An online algorithm repository for cancer image analysis.** ***Computer Methods and Programs in Biomedicine*****, 2011.**

[7] **G. M. et. al. Tozer. Disrupting tumour blood vessels.** ***N R Cancer*****, 5(6):423–35, 2005.**

[8] **G. M. Tozer** *et. al.* **. Mechanisms associated with tumor vascular etc.** ***Cancer Res*****, 61:6413–6422, 2001.**

[9] **G. M. Tozer** *et. al.* **. Blood vessel maturation etc.** ***Cancer Res.*****, 68(7):2301–2311, 2008.**

[10] **J. A. Tyrrell** *et. al.* **. Robust 3d model of vasc imag using superellipsoids.** ***IEEE TMI*****, 26(2):223–237, 2007.**